university of groningen / faculty of science and engineering

Aerodynamic influence of shark-skin inspired surface textures

Final report

Industrial Engineering and Management Integration Project

Author:
J. Veenhuizen
Student number: S4465083
28th of June, 2023

First supervisor:
prof. dr. A. (Antonis) Vakis
Second supervisor:
M. (Mehran) Mohebbi, MSc
Daily supervisor:
T.M. (Tim) Kousemaker, MSc

Abstract

The studies of biomimicry provide inspiration to researchers overcoming technical challenges by looking at nature. Sharkskin textured surfaces are a great example of this because they are able to reduce the experienced drag. In this paper, three different geometries inspired by this have been researched, namely the v-groove design, the sawtooth design, and the blade design. On these designs, multiple parameters have been tested. Using COMSOL Multiphysics simulations were carried out. To get the best results during the limited time frame of this research, the k-ε turbulence model was chosen for the simulations. Since the main property that sharkskin textures are known for is drag reduction, the drag coefficient of these simulations was retrieved relative to the surface area that makes contact with the flow. For all tested parameters an optimum has been found.

Contents

List of Figures

List of Tables

Chapter 1

Introduction

Once every two years the Bridgestone World Solar Challenge takes place in Australia. During this race, teams use the power of the sun to drive over 3,000 kilometers in solar cars [4]. To do this as fast as possible, teams strive to get their cars as light and efficient as achievable. An important factor for efficiency is the aerodynamic drag that is experienced. The influence of the shape of the cars on aerodynamics has been known for a long time and teams carefully take it into account when designing the cars. However, in recent years the potential influence of micro-scale surface texture on the drag has been brought up. In the 2019 edition, one team claimed to use this technique on their car [21]. Top Dutch Solar Racing wants to know if this sharkskin technology could reduce the air drag of their car.
The reduction of drag is an important factor in different fields. Before being banned in 2009, the technology was successfully implemented in swimming suits with 83% of the medals at the 2000 Olympics being won by swimmers using these suits [19]. Furthermore, in the aerospace industry sharkskin technology is being used to reduce fuel consumption. Even though the implementation is not yet widespread, many companies are testing the technology on their planes. This implementation could potentially save up to $1 million dollars per airplane in fuel consumption each year [23]. One method of manufacturing sharkskin textured surfaces is through 3D printing. Tests run on drag reduction of 3D-printed sharkskin-inspired surfaces have shown to reduce drag up to 9% [7]. Furthermore, one study combining polymer additives and sharkskin found a drag reduction rate of up to 80% [5]. The drastic difference could possibly be explained by the limitations of current 3D printing techniques. The precision of 3D printers is up to six times higher with 60 μm [24], compared to sharkskin denticle sizes as small as 10.5 μm [6].

The research outlined in this report could positively influence the air drag reduction on solar cars. Currently, the implementation of these techniques is not widespread in the industry. By researching multiple parameters for the surface texture, the implementation of this technique could be more achievable. The main research question of this project will be: *What set of parameter dimensions for sharkskin-like surface texture can be used to reduce air drag?* The following part of the report will analyze the problem, where literature will be used to support the theory. After this, a detailed design for the research will be outlined and the results will be analyzed. Lastly, a conclusion and future work will be discussed.

Chapter 2

Problem analysis

2.1 PROBLEM CONTEXT

The power needed to complete a solar race is depended on several factors, air drag is a controllable and important contributor [9]. This parameter is important in many fields of transportation. Since airflow behaves similarly at different altitudes, research on this topic is applicable to both land and air transportation [18]. In order to run simulations it is necessary to know in what flow regime it is operating, and thus its Reynolds number. To calculate this, the following formula can be used:

$$Re = \frac{\rho u L}{\mu} \tag{2.1}$$

where ρ is the density of the fluid, u is the flow speed, L is the characteristic linear dimension, and μ is the dynamic viscosity of the fluid. This research focuses on the flow characteristics at the shark-skin inspired denticles. Therefore, the characteristic linear dimension is that of these rigids. When using this to calculate the Reynolds number, it can be concluded that the resulting Reynolds number is in the low Reynolds number turbulence regime.

2.2 SYSTEM DESCRIPTION

The skin of sharks is covered in small denticles with heights as small as 10.5 μm and a density of up to 130 denticles per millimeter squared [6]. These denticles delay flow separation [8]. Flow separation negatively influences the drag experienced by a body [1]. Delaying the flow separation reduces the wake behind the object, and thus the drag [22]. These denticles have rigids in the flow direction. Figure 2.1 gives a representation of these denticles. The delay in flow separation can be explained by cavity vortices that appear at the denticles, making the water appear to skip over its body. This rough surface, however, does not directly cause the flow to become turbulent [11].

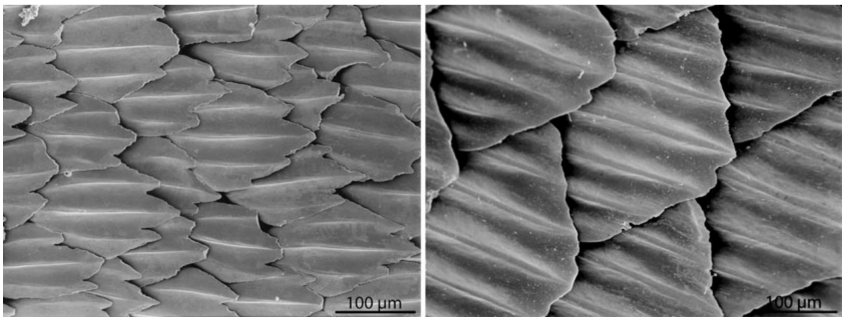

Figure 2.1: Scanning electron micrograph (200x) of the placoid scales of a short-fin mako shark Isurus oxyrinchus (left) and blacktip shark Carcharhinus limbatus (right) from the dorsal body wall anterior to the dorsal fin. The mako shark scale has three keels or riblets, whereas the blacktip shark has five. Anterior is to the left [10].

For the high and low-level systems of the car, the aerodynamics of the entire car can be seen as a high-level system and the surface texture as a low-level system. The flow field before making contact with the car is the input of the system. The resulting flow field when flowing around the car is the output of the system. At a low level, the input and output differ for each individual denticle, as the output of one denticle will be the input of the following. This report will focus on the low-level system. The altered flow at this low-level structure combined will influence the flow of the high-level system. The parameters influencing this low-level system are connected to the size of the rigids. A factor contributing to the flow is the angle of attack. This angle of attack is outside the scope of the low-level system.

Chapter 3

Theoretical background

3.1 Geometry

Different research conducted on sharkskin technology has shown that their geometry heavily influences the effect of the denticles.

One study comparing a blade design and a wedge design showed that the wedge design has a better drag reduction [25]. Furthermore, different parameters for this wedge design are discussed. These parameters include the height, the angle of the wedge, the curvature of the tip, and the curvature of the lower part of the wedge. The curvatures of the tip and the lower part of the wedge have been shown to negatively influence the drag reduction rate [25]. However, both the angle and the height of the wedge have been shown to drastically influence the drag reduction rate. The optimal height is found to be between 0.20 mm and 0.25 mm. The angle of the wedge showed to decrease the drag reduction rate when the angle was increased. The tests were performed between 15 $^\circ$ and 75 $^\circ$.

Other research comparing four different geometries found that all shapes have different drag reduction efficiencies [2]. This research compared v-shaped, sawtooth, rectangle-grooved, and semi-circular grooved designs. Both the v-shaped and sawtooth designs stood out in terms of the highest drag reduction properties. The sawtooth design produced the overall best reduction rates. However, the results of this sawtooth design also showed some fluctuations [2].

Besides the geometries, research about the influence of the aspect ratio (AR) between the height and width of the geometries has been conducted. The aspect ratio has been defined as $AR = 2H/W$ with H being the height of the geometry, and W as the width. When this AR is slightly below one, different geometries show the best drag reduction properties [16].

3.2 Flow separation

Flow separation is the phenomenon when a fluid, such as air, passing over an object fails to follow the curvature of the object. When a fluid flows over a surface, it experiences different forces, such as pressure and friction. Under normal conditions, the fluid adheres to the surface, flowing smoothly and following its shape. However, certain factors can disrupt this smooth flow, leading to flow separation [1].

Flow separation has significant effects on the aerodynamic performance of objects. It can lead to increased drag, reduced lift, and altered stability [1]. The area of low pressure behind the object grows when flow separates, resulting in a higher drag force. This increased resistance can be detrimental in various applications, such as airplanes and cars, as it requires additional energy to overcome the drag and maintain the desired speed.

Delaying flow separation hence decreasing its effect. Thus, delaying the flow separation reduces the drag.

Chapter 4

Research design

To research the influence of different parameters of sharkskin denticles on aerodynamics, a number of simulations are executed using COMSOL Multiphysics. In Chapter 2, it is found that the simulations take place in the low Reynolds number turbulence regime. Taking this regime into account and considering the lower computational power compared to other models, the k-ε turbulence model was selected.

The simulations are focused on the effect of multiple geometries as well as the effect of the size of the rigids relative to the body. The drag coefficient of these designs is evaluated after the simulation and compared to a control setup. This control setup consists of an empty box with one surface that depicts the surface of a body without sharkskin textures.

Table 4.1: Computer specifications

CPU	Intel(R) Core(TM) i7-10510U @ 2.5 GHz
Cores	4 Cores, 8 Threads
RAM	16 GB DDR3 @ 2133 MHz
GPU	Nvidia GeForce MX250

The following parts discuss the different parameters that were tested, how these parameters were tested, how the models have been set up, and how the drag coefficient was calculated. The simulations were executed on a Huawei Matebook X Pro. In Table 4.1 the specifications of this laptop can be seen. The total run time of all nine simulations combined resulted is roughly 75 hours and 20 minutes.

4.1 Parameters

During the research, five parameters that influence the drag-reducing properties of sharkskin denticles have been simulated. The following section discusses these parameters and explains how their effects were tested. The parameters looked into during the simulations are:

1. Shape

2. Aspect Ratio
3. Size
4. Inlet Geometry
5. Relative Positioning.

4.1.1 Shape

Based on findings in literature, three promising shape designs have been selected. These shapes will be referred to as the v-groove, sawtooth, and blade design. In Figure 4.1 2D views of the designs can be seen, where W is the width and H is the height of the denticles. The influence of the geometry was researched by comparing the results of the simulations for the other parameters. Since the setup for the different simulations is the same, differences between the simulations on the same parameter say something about the effect of the geometry.

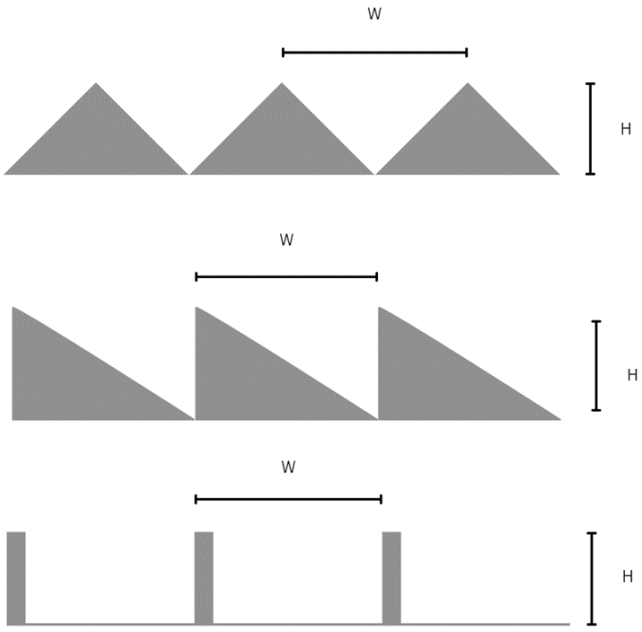

Figure 4.1: Front views of the three different designs, the top one being the v-groove desing, the middle one the sawtooth design, and the bottom one the blade design

4.1.2 Aspect Ratio

The influence of aspect ratio is discussed in multiple papers. It is found that for each Reynolds number there is an optimal aspect ratio [12, 17]. One study found that the optimal aspect ratio is close to AR ≈ 1, where AR is defined as $AR = \frac{2A}{\lambda}$ [16]. In this formula AR is the aspect ratio, with A as the amplitude and λ as the wavelength. For this research, AR is defined as $AR = \frac{2H}{W}$ as discussed in Chapter 3. This parameter is tested by performing a parametric sweep, where the rigid width is constant and the rigid height is changed. In doing so, the aspect ratio takes the following values: AR=0.5, AR=1, AR=1.5, and AR=2.

4.1.3 Size

The size of the denticles is tested by changing the height and width of the denticles with the same factor. By changing the size with a relative factor, the aspect ratio is equal and therefore it does not influence the effect. The aspect ratio is set to AR=1 during this test as research by Raayai-Ardakani and McKinley [16] has shown this to be close to the optimum aspect ratio for different geometries and Reynolds numbers. Through the implementation of a parametric sweep, the rigid width is set to take the following values: 15 μm, 30 μm, 45 μm, and 90 μm. Due to the constant aspect ratio, the rigid height is half of the rigid width. All other variables such as the rigid length, stay constant between all simulations.

4.1.4 Inlet Geometry

One study on the effect of inclined inlet angles on shark-skin denticles showed that the angle of these denticles influences the drag coefficient [15]. Through a parametric sweep, an inlet angle of 7.5°, 15°, 30°, 45°, and 60°is tested. This simulation is only done for the v-groove design. The choice to test this parameter on only one geometry is due to the limited time frame of this study combined with the computational power needed to run the simulations. The v-groove design is selected as the internal COMSOL geometry options allow for easier implementation of this inclined inlet compared to the other designs.

4.1.5 Relative Positioning

The final parameter that is tested is the relative position. This test looks into how the denticles are placed relative to one another. There are three options that were tested. The first option is a continuous configuration, where the denticles run from the front to the back and are placed directly next to one another. The second option is a staggered configuration, where the denticles are placed in a chessboard

pattern. The final option is a grouped staggered configuration. In this configuration, the continuous and staggered configurations are combined to have groups of denticles placed directly beside each other in a chessboard pattern. It has been found that both the staggered and continuous configuration can outperform the other at different Reynolds numbers [3]. The first configuration is implemented in the tests for all the other parameters. Both other configurations were only run for the v-groove design. For the staggered configuration, a parametric sweep on the rigid length is conducted. These rigid lengths take the following values: 50 μm, 100 μm, 200 μm, and 500 μm. For the grouped configuration, a rigid length of 250 μm is used. The group size is tested for groups of 3, 5, 10, and 15 denticles placed adjacent to each other.

4.2 Model setup

To ensure that the outcome of the different simulations can be compared, all settings regarding the size, input values, wall settings, and mesh have been set to the same value. These settings will be discussed first, followed by the individual differences between the different tests.

4.2.1 Input values

The entire geometry is set to be a box with a width of 750 μm, a height of 3 mm, and a length of 10 mm. These dimensions offer enough space for the test region to generate results without interference from the walls. The front of the geometry is set as the input with a velocity of 20 m/s. This velocity has been selected as this is roughly the average speed of the solar cars during the challenge. The rear of the box has been set as the outlet. All walls at the top and sides of the setup have been set to a slip condition. This slip setting assumes the walls induce no viscous effects. Because of this no boundary layer forms and therefore, the only function of these walls is to prevent the air from leaving the domain [20]. The surface that is tested has the same width as the box and a length of 5 mm. This surface is placed at 500 μm from the inlet. This small space in front of the test area offers enough space for the flow to not interfere with itself and influence the results. The surface area of this region is set to a no-slip condition.

4.2.2 Mesh

The test domain has been split up into different sections. These different sections have been created in order to allow for different mesh sizes in different parts. This makes it possible to reduce the computational power while still getting accurate

results. In Figure 4.2 the difference between the mesh size per domain can be seen. The built-in COMSOL user-controlled mesh has been used to create the mesh. Three different domain mesh settings are introduced and calibrated for fluid dynamics. The domains at the top are all set to extra coarse, as the main function of this region is to have enough space between the test surface and the walls at the top. At the bottom, both regions located at the sides are set to a normal mesh. Part of the function of these regions is to allow the flow to be free from interference. Due to the growth settings, which depict how much difference in size is allowed between neighboured nodes, the most important sections of these domains are more precise than the region closest to the output. The final domain is the part where the test surface is placed. This region is set to the fine mesh setting. Furthermore, the surface area of this region is also set to a fine setting.

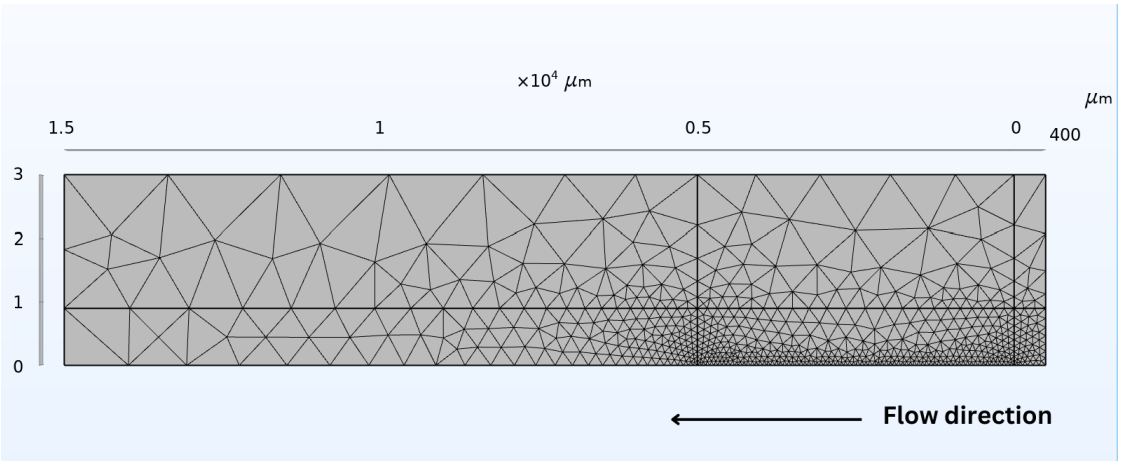

Figure 4.2: Setup of the mesh in the control situation

4.3 Drag coefficient

The performance of relative designs and parameters is evaluated based on the drag coefficient. This coefficient is a dimensionless number and is calculated using the following formula:

$$c_{\mathrm{d}} = \frac{2F_{\mathrm{d}}}{\rho u^2 A} \tag{4.1}$$

where F_{d} is the total drag force, ρ the mass density of air, u the flow speed, and A the reference area. This reference area can be calculated in two different ways [14]. It is important to note that these two methods can generate different outcomes for the same situation. Therefore, it is not possible to compare the

outcomes of the different definitions. The first option is to take the area normal to the flow direction. However, this introduces a problem for the control situation. In this situation, there is no area normal to the flow direction. Since dividing by zero is not possible, this choice for the area makes it impossible to calculate the drag coefficient for the control situation. The second option is to take the entire surface area that makes contact with the flow. This makes it possible to calculate the drag coefficient for all simulations. Therefore, this definition for A has been selected. To retrieve the total drag force in COMSOL, some built-in functions have been used. First, using the integral function all surfaces of the geometry are selected. Using "variables" the area can be retrieved from the integral using the internal operator. The flow speed is equal to the input velocity and the mass density of air is known. This leaves the total drag force, which can be retrieved from the integration as well. This can be done by using the expression *spf.nymesh * p + spf.rho * spf.u_tau * spf.u_tangy / spf.uPlus* [13]. The calculated drag coefficient can be retrieved using derived values after running the simulation.

Chapter 5

Results

The following parts will discuss the results. The results are split up into three sections; the aspect ratio, the size, and the inlet geometry & relative positioning. The results are presented as the drag coefficient over the tested parameter.

5.1 Aspect Ratio

In Figure 5.1 it can be seen that the three different geometries all follow a similar pattern regarding the drag coefficient. Even though all designs show to outperform the control situation, there is still a noticeable difference between the designs. Furthermore, it can be seen in Table 5.1 as well as in the figure that all designs have an optimum at an aspect ratio of two. This contradicts the findings in the literature, where it is found that this optimum is around an aspect ratio of one.

Table 5.1: Drag coefficients for all designs at different aspect ratios

	V-GROOVE	**SAWTOOTH**	**BLADE**	**CONTROL**
Aspect Ratio [-]	Drag Coefficient [-]	Drag Coefficient [-]	Drag Coefficient [-]	Drag Coefficient [-]
1/2	1.0319e-2	0.9523e-2	0.9422e-2	1.1216e-2
1	1.0037e-2	0.9179e-2	0.9118e-2	1.1216e-2
1 1/2	1.0146e-2	0.9312e-2	0.9177e-2	1.1216e-2
2	1.0035e-2	0.8999e-2	0.8884e-2	1.1216e-2

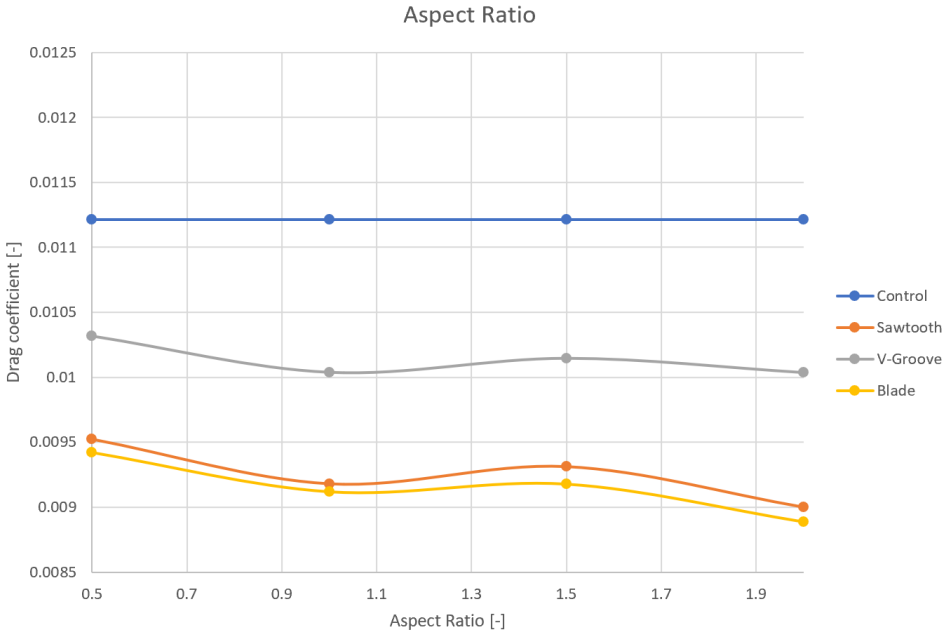

Figure 5.1: Graph of the resulting drag coefficients for the designs at different aspect ratios

5.2 Size

In Figure 5.2 it can be seen that both the sawtooth and the v-groove design show similar behavior regarding the size. It can be seen that these designs are not beneficial for all denticle sizes. For the v-groove design, this moment comes at roughly 70 μm and for the sawtooth design, this moment comes shortly after 77 μm. However, the blade design deviates strongly from the pattern shown by the other designs and shows to outperform the control situation for all tested sizes. Even though not all designs show the same behavior, it can be seen that regardless of the design, the shortest tested rigid width results in the lowest drag coefficient.

Table 5.2: Drag coefficients for all designs at different sizes

	V-GROOVE	**SAWTOOTH**	**BLADE**	**CONTROL**
Rigid width [μm]	Drag Coefficient [-]	Drag Coefficient [-]	Drag Coefficient [-]	Drag Coefficient [-]
15	0.9484e-2	0.9493e-2	0.8997e-2	1.1216e-2
30	1.0106e-2	1.0027e-2	0.9028e-2	1.1216e-2
45	1.0556e-2	1.0465e-2	0.9063e-2	1.1216e-2
90	1.1765e-2	1.1533e-2	0.9023e-2	1.1216e-2

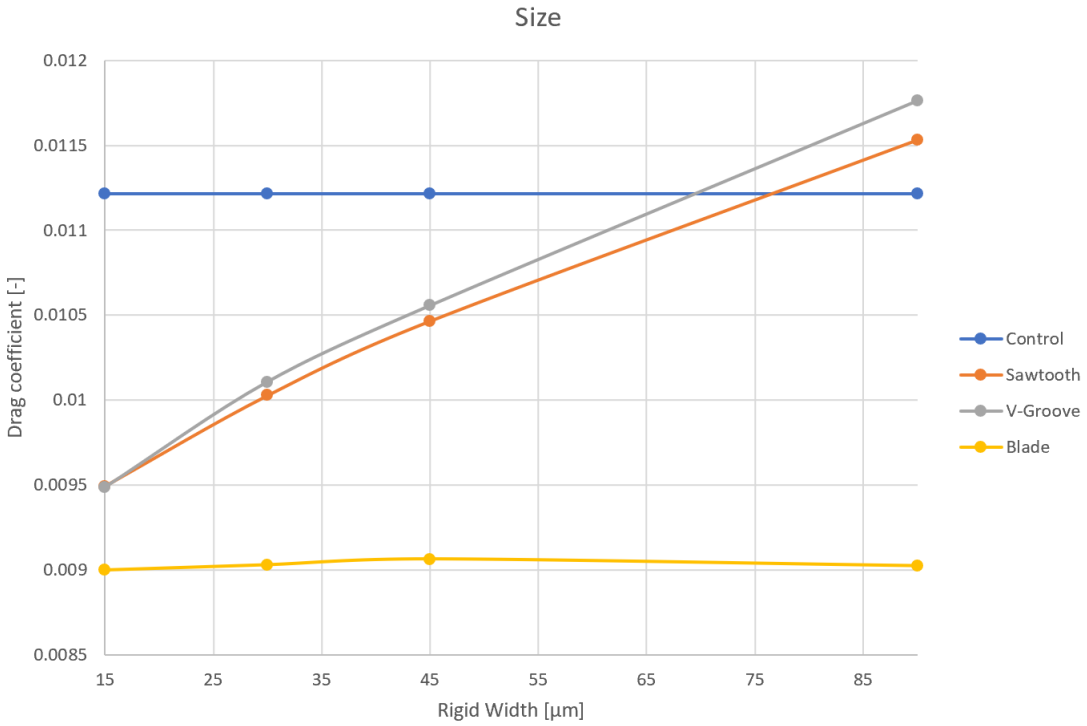

Figure 5.2: Graph of the resulting drag coefficients for the designs at different sizes

5.3 Inlet Geometry & Relative Positioning

Tables 5.3, 5.4, and 5.5 show the test results for the inlet and configuration tests. For the inlet angle, it can be seen that there is an optimum at a 30-degree angle. In sections 5.1 and 5.2 for AR=1 and Rigid width=30 μm respectively, the v-groove design has the same size without a sloped inlet. It can be seen that the drag coefficient, in these cases, is roughly 0.010. When comparing this to any of

the results with a sloped inlet, it can be seen that having an inlet angle results in a lower drag coefficient.

Table 5.3: Drag coefficient for the different inlet angles

Angle [deg]	7.5	15	30	45	60
Drag coefficient [-]	0.9658e-2	0.9359e-2	0.9333e-2	0.9593e-2	0.9753e-2

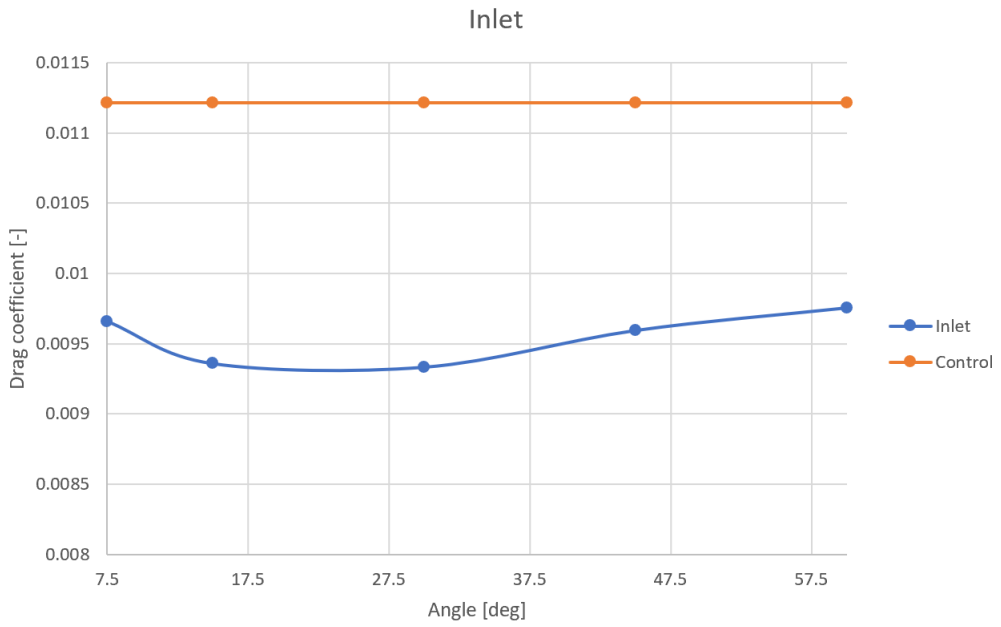

Figure 5.3: Graph of the drag coefficient at different inlet angles

In Table 5.4 it is notable that the different drag coefficient differ much more from one another respective to the other tests. Furthermore, it is remarkable that the drag coefficient is roughly a tenth of the control situation for a rigid length of 50 μm.

Table 5.4: Drag coefficient for different rigid lengths in the alternated design

Rigid length [μm]	50	100	200	500
Drag coefficient [-]	0.1240e-2	0.2174e-2	0.3052e-2	0.6631e-2

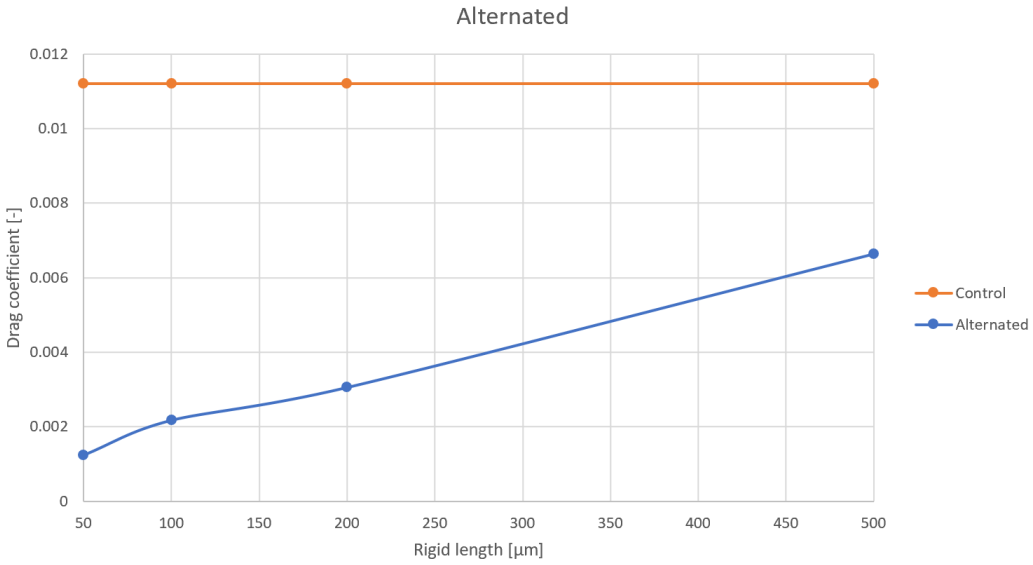

Figure 5.4: Graph of the drag coefficient at different rigid lengths

In Table 5.5 it can be seen that the higher the number of denticles in a group, the higher the resulting drag coefficient is. This trend can also be continued by the results of the alternated configuration. The grouped design has been simulated with a rigid length of 250 μm. For the alternated configuration this length has not been tested. However, when looking at the curve of the drag coefficient in Figure 5.4, it can be seen that the resulting drag coefficient would be below 0.0040 at this rigid length.

Table 5.5: Drag coefficient for different numbers of denticles directly next to one another in the alternated design

Groups [-]	3	5	10	15
Drag coefficient [-]	0.6179e-2	0.6548e-2	0.6989e-2	0.7327e-2

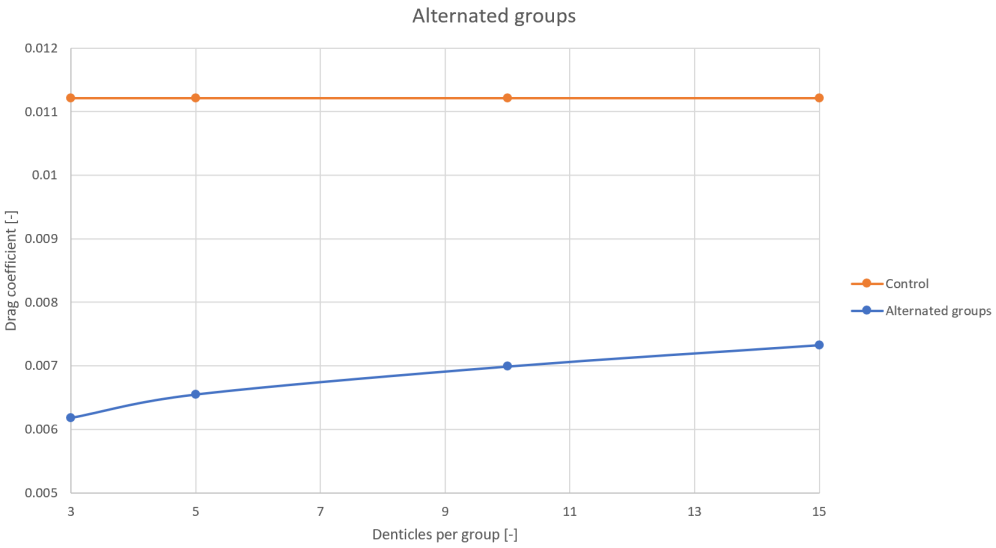

Figure 5.5: Graph of the drag coefficient at different group sizes

Chapter 6

Discussion

In order to validate the results, two simulations have been run at a higher-order discretization. Both the alternated and the alternated group designs have been simulated at a higher order. In Tables 6.1 and 6.2 both the resulting drag coefficient for the simulations used during this research, as well as the results for the higher order discretization have been displayed.

Table 6.1: Drag coefficient for different numbers of denticles directly next to one another in the alternated design. The top row reports the results of the simulation used during the research. The bottom row reports the results of a simulation run at a higher order.

Groups [-]	3	5	10	15
Drag coefficient [-]	0.6179e-2	0.6548e-2	0.6989e-2	0.7327e-2
Drag coefficient higher order [-]	0.7751e-2	0.7974e-2	0.8096e-2	0.8222e-2

Table 6.2: Drag coefficient for different rigid lengths in the alternated design. The top row reports the results of the simulation used during the research. The bottom row reports the results of a simulation run at a higher order.

Rigid length [m]	50	100	200	500
Drag coefficient [-]	0.1240e-2	0.2174e-2	0.3053e-2	0.6631
Drag coefficient higher order [-]	0.4155e-2	0.5946e-2	0.6189e-2	0.7759e-2

As can be seen in Table 6.1, the results differ between them by up to 20%. However, the higher the number of denticles placed in a group, the closer the results get to one another. This inaccuracy can be explained by the mesh size compared to the size of the denticles. It is important to note that this inaccuracy influences the results of all simulations. Most importantly, the simulations with the smallest elements, such as the alternated design with a rigid length of 50 μm. The difference in results between both orders of discretization reduces as the size of the denticles grows. This decrease in difference can be seen in Figure 6.1. In Figure 6.2 it can be seen that the trend of the alternated group simulations at different order discretizations is similar.

Another limitation of this research is the definition of friction. As explained in Chapter 4, the test surface has been set to a no-slip condition. This method has its limitations when it comes to accurately simulating the body of a solar car.

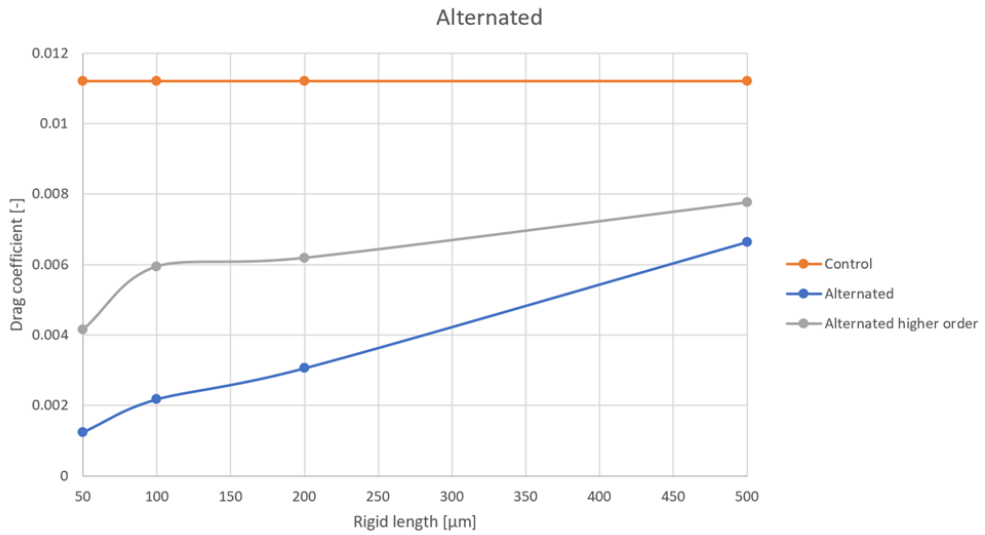

Figure 6.1: Graph of the drag coefficient at different orders of discretization for the alternated configuration

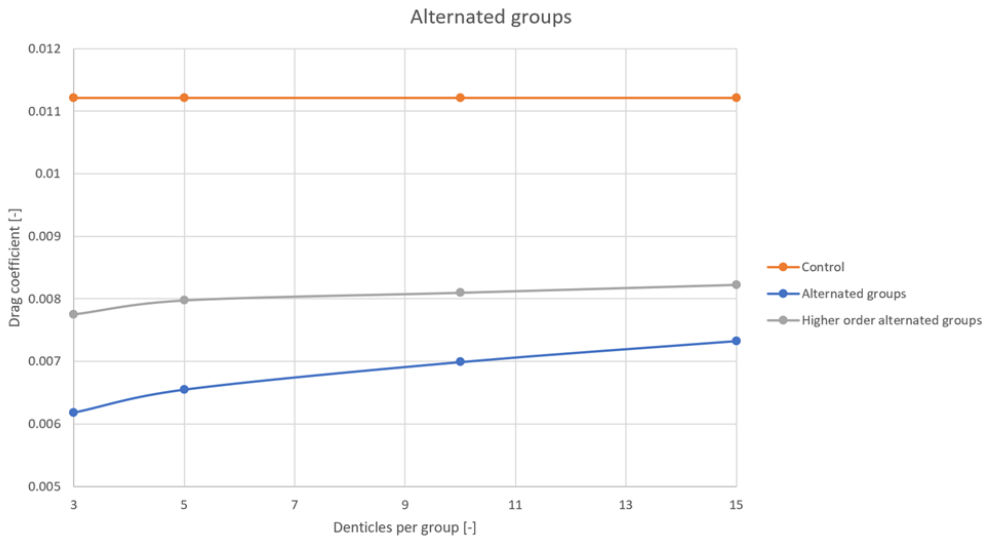

Figure 6.2: Graph of the drag coefficient at different orders of discretization for the alternated group configuration

Chapter 7

Conclusion

In Chapter 5 it can be seen that the tests show that all tested parameters can reduce the drag coefficient. All tested parameters have been shown to have an optimum. The maximum size before increasing the drag coefficient relative to the control situation has been shown to be dependent on the design. However, it can also be concluded that the smaller the size, the better the drag coefficient for the tested range of sizes. Regarding the configuration of the denticles, it has been shown that the alternated design outperforms the grouped alternated design and the continuous design noticeably. Furthermore, it is found that in this alternated design shorter rigid lengths outperform longer rigid lengths. The optimal aspect ratio shows to differ from the findings in the literature, which could be caused by the difference in the definition of the reference area. At AR=2, this optimum is found. The inlet angle has been shown to have an effect on drag reduction. The optimum for this angle is 30 degrees. Furthermore, it can be concluded that the different designs show similar behavior. There is one exception to this, the blade design for the size simulation. This difference could be caused by inaccuracies during the simulation. However, it could also indicate that for some geometries the influence of size follows a different trend line. When combining the different optima in one design will result in an alternated design with a rigid length of 50 μm, a rigid width of 15 μm, an AR of 2, and an inlet angle of 30 °. For the geometry, this study would suggest the blade design would yield the best results. However, it can be argued that such a design would be vulnerable and could easily break when implemented. Therefore, the sawtooth design might be a better choice, as it has been shown to perform comparably to the blade design.

7.1 Future work

In future studies, the effect of the denticles should be tested when the inlet angle of the flow alters. In real-world situations, the airflow will not always come normal to the denticles. When implemented in the real world, fouling will become another factor. The effects and characteristics of different geometries on fouling should be researched. Besides this, it should be tested how these parameters influence one another. For example by implementing a sloped inlet on the alternated design. Furthermore, adding denticles to an object adds weight. The reduction in drag should be compared to the increased weight. Lastly, the overall drag-reducing effects of these denticles should be investigated when placed on an object.

Chapter 8

References

[1] Anderson, John David. *Fundamentals of aerodynamics*. 6th ed. Columbus, OH: McGraw-Hill Education, 2016.

[2] Qingshun Bai et al. "Drag reduction characteristics and flow field analysis of textured surface". In: *Friction* 4 (2016), pp. 165–175.

[3] Gregory D Bixler and Bharat Bhushan. "Fluid drag reduction with shark-skin riblet inspired microstructured surfaces". In: *Advanced Functional Materials* 23.36 (2013), pp. 4507–4528.

[4] World Solar Challenge. *World Solar Challenge 2023*. URL: https://worldsolarchallenge.org/.

[5] Huawei Chen et al. "Synthetic effect of vivid shark skin and polymer additive on drag reduction reinforcement". In: *Advances in Mechanical Engineering* 6 (2014), p. 425701.

[6] Hsiu-Wen Chien et al. "Inhibition of biofilm formation by rough shark skin-patterned surfaces". In: *Colloids and Surfaces B: Biointerfaces* 186 (2020), p. 110738.

[7] Wei Dai et al. "Drag-reduction of 3D printed shark-skin-like surfaces". In: *Friction* 7 (2019), pp. 603–612.

[8] Pengming Guo et al. "On the influence of biomimetic shark skin in dynamic flow separation". In: *Bioinspiration & Biomimetics* 16.3 (2021), p. 034001.

[9] Najib A. Kasti. "Ranges of applicability of a solar-battery car with single and double solar-trailers". In: *SOLAR ENERGY* 144 (Mar. 2017), pp. 619–628. ISSN: 0038-092X. DOI: 10.1016/j.solener.2017.01.051.

[10] Amy Lang, Maria Laura Habegger, and Philip Motta. "Shark skin drag reduction". In: *Encyclopedia of nanotechnology* 19 (2012), pp. 2394–2400.

[11] AW Lang et al. "Bristled shark skin: a microgeometry for boundary layer control?" In: *Bioinspiration & biomimetics* 3.4 (2008), p. 046005.

[12] Kangmei Li et al. "Numerical investigation of the tribological performance of micro-dimple textured surfaces under hydrodynamic lubrication". In: *Beilstein journal of nanotechnology* 8.1 (2017), pp. 2324–2338.

[13] P. Lyu. *How Do I Compute Lift and Drag?* June 2015. URL: https://www.comsol.com/blogs/how-do-i-compute-lift-and-drag/.

[14] NASA. *The Drag Equation*. URL: https://www.grc.nasa.gov/www/k-12/rocket/drageq.html#:~:text=If%20we%20think%20of%20drag,perpendicular%20to%20the%20flow%20direction..

[15] Fernandez-Waid Patricia et al. "Morphological characterization and hydrodynamic behavior of shortfin mako shark (Isurus oxyrinchus) dorsal fin denticles". In: *Journal of Bionic Engineering* 16 (2019), pp. 730–741.

[16] Shabnam Raayai-Ardakani and Gareth H McKinley. "Drag reduction using wrinkled surfaces in high Reynolds number laminar boundary layer flows". In: *Physics of Fluids* 29.9 (2017), p. 093605.

[17] Shabnam Raayai-Ardakani and Gareth H McKinley. "Geometric optimization of riblet-textured surfaces for drag reduction in laminar boundary layer flows". In: *Physics of Fluids* 31.5 (2019), p. 053601.

[18] Faiza Shahid et al. "Variation in aerodynamic coefficients with altitude". In: *Results in Physics* 7 (2017), pp. 1261–1273. ISSN: 2211-3797. DOI: https://doi.org/10.1016/j.rinp.2017.03.020. URL: https://www.sciencedirect.com/science/article/pii/S2211379717302437.

[19] Ray Stefani. "Olympic Swimming Gold: The Suit or the Swimmer in the Suit?" In: *Significance* 9.2 (Apr. 2012), pp. 13–17. ISSN: 1740-9705. DOI: 10.1111/j.1740-9713.2012.00553.x. URL: https://doi.org/10.1111/j.1740-9713.2012.00553.x.

[20] *Theory for the Wall Boundary Condition*. COMSOL Multiphysics. URL: https://doc.comsol.com/5.5/doc/com.comsol.help.cfd/cfd_ug_fluidflow_single.06.065.html.

[21] Vattenfall. *Geheim wapen Vattenfall Solar Team onthuld: shark skin;* Aug. 2019. URL: https://group.vattenfall.com/nl/newsroom/persbericht/2019/geheim-wapen-vattenfall-solar-team-onthuld-shark-skin.

[22] Haipeng Wang et al. "Effects of leading edge slat on flow separation and aerodynamic performance of wind turbine". In: *Energy* 182 (2019), pp. 988–998.

[23] Guijian Xiao et al. "Shark-skin-inspired micro-riblets forming mechanism of TC17 titanium alloy with belt grinding". In: *Ieee Access* 7 (2019), pp. 107635–107647.

[24] Yuji Yasuda et al. "Manufacturing of biomimetic silicone rubber films for experimental fluid mechanics: 3D printed shark skin molds". In: *Journal of The Electrochemical Society* 166.9 (2019), B3302.

[25] Hai-Yan Yu et al. “Thermodynamic analysis of shark skin texture surfaces for microchannel flow”. In: *Continuum Mechanics and Thermodynamics* 28 (2016), pp. 1361–1371.